J|A|C|S ARTICLES

Published on Web 06/10/2009

# Optimization of FeMoco Maturation on NifEN

Janice M. Yoshizawa,[†] Michael A. Blank,[‡] Aaron W. Fay,[†] Chi Chung Lee,[†] Jared A. Wiig,[†] Yilin Hu,*[,†] Keith O. Hodgson,*[,‡,§] Britt Hedman,*[,§] and Markus W. Ribbe*[,†]

*Department of Molecular Biology and Biochemistry, University of California, Irvine, California 92697, Department of Chemistry, Stanford University, Stanford, California 94305, and Stanford Synchrotron Radiation Lightsource (SLAC), Stanford University, Menlo Park, California 94025*

Received March 10, 2009; E-mail: yilinh@uci.edu; hodgson@ssrl.slac.stanford.edu; hedman@ssrl.slac.stanford.edu; mribbe@uci.edu

***Abstract:*** Mo-nitrogenase catalyzes the reduction of dinitrogen to ammonia at the cofactor (i.e., FeMoco) site of its MoFe protein component. Biosynthesis of FeMoco involves NifEN, a scaffold protein that hosts the maturation of a precursor to a mature FeMoco before it is delivered to the target location in the MoFe protein. Previously, we have shown that the NifEN-bound precursor could be converted in vitro to a fully complemented "FeMoco" in the presence of 2 mM dithionite. However, such a conversion was incomplete, and Mo was only loosely associated with the NifEN-bound "FeMoco". Here we report the optimized maturation of the NifEN-associated precursor in 20 mM dithionite. Activity analyses show that upon the optimal conversion of precursor to "FeMoco", NifEN is capable of activating a FeMoco-deficient form of MoFe protein to the same extent as the isolated FeMoco. Furthermore, EPR and XAS/EXAFS analyses reveal the presence of a tightly organized Mo site in NifEN-bound "FeMoco", which allows the observation of a FeMoco-like $S = {}^3/_2$ EPR signal and the modeling of a NifEN-bound "FeMoco" that adopts a conformation very similar to that of the MoFe protein-associated FeMoco. The sensitivity of FeMoco maturation to dithionite concentration suggests an essential role of redox chemistry in this process, and the optimal potential of dithionite solution could serve as a guideline for future identification of in vivo electron donors for FeMoco maturation.

## 1. Introduction

Nitrogenase provides the biochemical machinery for ATP-dependent reduction of $N_2$ to $NH_3$. The best-characterized Mo-nitrogenase[1] is a binary system comprising the Fe protein and the MoFe protein. The Fe protein is an $\alpha_2$-homodimer containing one $[Fe_4S_4]$ cluster at the subunit interface and one MgATP binding site in each subunit, whereas the MoFe protein is an $\alpha_2\beta_2$-heterotetramer containing one P cluster ($[Fe_8S_7]$) at each $\alpha/\beta$-subunit interface and one FeMoco ($[MoFe_7S_9X-$homocitrate], where X = C, N, or O) within each $\alpha$ subunit. Nitrogenase catalysis involves repeated association and dissociation of the Fe and MoFe proteins and ATP-hydrolysis-driven interprotein electron transfer from the $[Fe_4S_4]$ cluster of the Fe protein to the P cluster and then to the FeMoco of the MoFe protein, where substrate reduction occurs.

Biosynthesis of FeMoco[2] is presumably launched by the production of an Fe/S core structure on NifB (encoded by *nifB*), which is then transferred to NifEN (encoded by *nifE* and *nifN*) for further processing before it is delivered to its target location in the MoFe protein. NifEN shares significant homology with the MoFe protein in primary sequence and cluster sites. It has been proposed that NifEN contains a "P cluster site" that houses a P cluster homologue and a "FeMoco site" that hosts the conversion of FeMoco precursor to a mature cluster.[2] Previously, we confirmed the identity of a P cluster homologue as an $[Fe_4S_4]$-type cluster and furthermore identified a FeMoco precursor as a Mo/homocitrate-free cluster that closely resembled the Fe/S core of FeMoco.[3,4] Subsequently, we showed that in an ATP- and reductant-dependent process, the Fe protein inserted Mo and homocitrate into the precursor, leading to the formation of a "FeMoco" on NifEN that could directly activate the FeMoco-deficient MoFe protein.[5,6] While these studies have established the key components of FeMoco assembly, a detailed molecular analysis of this process has remained elusive because of the lack of means to quantitatively obtain a fully matured form of NifEN-bound FeMoco. Our data indicated that conversion of precursor was incomplete in 2 mM dithionite, as the MoFe protein reconstituted by such a NifEN-bound "FeMoco" species was only ~30% as active as that by isolated FeMoco. Additionally, we were unable to unambiguously define the

[†] University of California, Irvine.
[‡] Stanford University.
[§] Stanford Synchrotron Radiation Lightsource.

(1) Burgess, B. K.; Lowe, D. J. *Chem. Rev.* **1996**, *96*, 2983–3012.
(2) Hu, Y.; Fay, A. W.; Lee, C. C.; Yoshizawa, J.; Ribbe, M. W. *Biochemistry* **2008**, *47*, 3973–3981.
(3) Hu, Y.; Fay, A. W.; Ribbe, M. W. *Proc. Natl. Acad. Sci. U.S.A.* **2005**, *102*, 3236–3241.
(4) Corbett, M. C.; Hu, Y.; Fay, A. W.; Ribbe, M. W.; Hedman, B.; Hodgson, K. O. *Proc. Natl. Acad. Sci. U.S.A.* **2006**, *103*, 1238–1243.
(5) Hu, Y.; Corbett, M. C.; Fay, A. W.; Webber, J. A.; Hodgson, K. O.; Hedman, B.; Ribbe, M. W. *Proc. Natl. Acad. Sci. U.S.A.* **2006**, *103*, 17119–17124.
(6) Hu, Y.; Corbett, M. C.; Fay, A. W.; Webber, J. A.; Hodgson, K. O.; Hedman, B.; Ribbe, M. W. *Proc. Natl. Acad. Sci. U.S.A.* **2006**, *103*, 17125–17130.

  

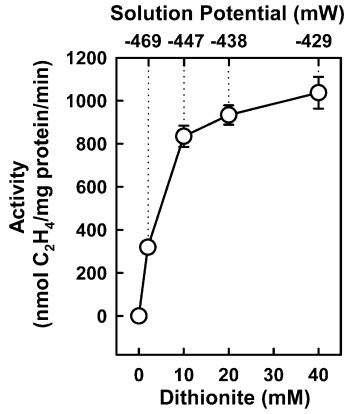


***Figure 1.*** Dithionite dependence of precursor maturation on NifEN. $NifEN^{Precursor}$ was first converted to $NifEN^{"FeMoco"}$ in varying concentrations of dithionite (0, 2, 10, 20, and 40 mM), and subsequently, $NifEN^{"FeMoco"}$ was reisolated and used as a FeMoco source for the reconstitution of FeMoco-deficient Δ*nifB* MoFe protein. Shown are the specific $C_2H_2$-reducing activities of MoFe protein upon reconstitution with $NifEN^{"FeMoco"}$ prepared at different dithionite concentrations. The calculated solution potentials[9] are indicated.

pattern of Mo binding on the basis of our X-ray absorption spectroscopy (XAS)/extended X-ray absorption fine structure (EXAFS) data, as Mo appeared to be only loosely associated to this "FeMoco".[5] Clearly, a reconstitution system that facilitates the complete formation of active FeMoco needs to be developed for the elucidation of the molecular details of FeMoco biosynthesis.

Here we report the optimization of FeMoco maturation on NifEN at an elevated reductant concentration (i.e., 20 mM dithionite), which not only suggests a key role of redox chemistry in this process but also permits the first detailed structural analysis of the NifEN-associated FeMoco species. Together, these studies constitute an important step toward establishing the mechanism of FeMoco assembly, which is one of the most outstanding questions in the field of metalloprotein biochemistry.

## 2. Results and Discussion

Three forms of NifEN were used in this study. One, designated as Δ*nifB* NifEN, contains two permanent $[Fe_4S_4]$ clusters but no FeMoco precursor because of the deletion of the *nifB* gene. Another, designated as $NifEN^{Precursor}$, contains a FeMoco precursor in addition to the two $[Fe_4S_4]$ clusters. The third, designated as $NifEN^{"FeMoco"(20mM)}$, contains a "FeMoco" matured in 20 mM dithionite. The elevated dithionite concentration allows the optimal conversion of precursor to "FeMoco" (Figure 1), as $NifEN^{"FeMoco"(20mM)}$ is capable of activating the FeMoco-deficient MoFe protein to the same extent as the isolated FeMoco (Table 1). Such a dramatic increase is not observed when the NifEN-bound precursor is matured in the absence of homocitrate (data not shown), suggesting that the matured cluster on NifEN is fully complemented with both Mo and homocitrate.

Consistent with the significant improvement in its reconstitution capacity, $NifEN^{"FeMoco"(20mM)}$ displays electron paramagnetic resonance (EPR) features (Figure 2; also see Figures S1 and S2 in the Supporting Information) that were not directly observed following the maturation of the precursor in 2 mM dithionite (designated as $NifEN^{"FeMoco"(2mM)}$ in the following text).[5] In the dithionite-reduced state, $NifEN^{"FeMoco"(20mM)}$ exhibits an $S = {}^3/_2$ EPR signal with $g$ values of 4.45, 3.96, and 3.60 at 6 K that is absent from the spectra of both Δ*nifB* NifEN and $NifEN^{Precursor}$ (Figure 2A). In addition, a new $g = 2.03$ feature appears in the $S = {}^1/_2$ signal of $NifEN^{"FeMoco"(20mM)}$ (Figure 2A). Clearly, the additional features in both the $S = {}^3/_2$ and $S = {}^1/_2$ regions of the $NifEN^{"FeMoco"(20mM)}$ spectrum are intimately associated with the attachment of Mo and homocitrate to the NifEN-bound precursor. Furthermore, the appearance of a FeMoco-like $S = {}^3/_2$ signal indicates the presence of a "FeMoco" species in NifEN that is very similar to the native FeMoco in the MoFe protein.

In the indigodisulfonate (IDS)-oxidized state, $NifEN^{Precursor}$ shows a distinct $g = 1.92$ signal at 15 K that is absent from the spectrum of the precursor-free Δ*nifB* NifEN (Figure 2B). This precursor-specific signal disappears in the case of $NifEN^{"FeMoco"(20mM)}$, suggesting a change in the electronic properties of the cluster upon insertion of Mo and homocitrate (Figure 2B). Interestingly, while the broad $g = 4.45$ and 3.60 features of $NifEN^{"FeMoco"(20mM)}$ disappear upon oxidation, the $g = 3.96$ and 2.03 features remain intact (Figure 2B). Thus, the Mo/homocitrate-associated features of $NifEN^{"FeMoco"(20mM)}$ do not always behave in sync, particularly those in the $S = {}^3/_2$ region (i.e., the features at $g = 4.45$, 3.96, and 3.60). This observation suggests that, unlike the $S = {}^3/_2$ signal of MoFe protein-associated FeMoco, the $S = {}^3/_2$ signal of NifEN-bound "FeMoco" may be generated by a mixture of $S = {}^3/_2$ species, likely reflecting its interactions with a cofactor site that is homologous to yet different than that in the MoFe protein.[2] Indirect support for this argument is provided by the EPR properties of FeVco, another FeMoco homologue that exhibits an $S = {}^3/_2$ signal with mixed composition.[7]

XAS/EXAFS spectroscopy of $NifEN^{"FeMoco"(20mM)}$ provides further structural proof that the "FeMoco" on NifEN closely resembles the native FeMoco in the MoFe protein (designated as $MoFe\ protein^{FeMoco}$) but has some unique features of its own. The Mo K-edge XAS spectra of $NifEN^{"FeMoco"(20mM)}$ and $MoFe\ protein^{FeMoco}$ show no difference in energy in the rising edge (Figure 3A) and a strong similarity in shape in the second derivative (Figure 3B), indicating that the effective charge and electronic environment of Mo in $NifEN^{"FeMoco"(20mM)}$ are very close to those in $MoFe\ protein^{FeMoco}$. In contrast, $NifEN^{"FeMoco"(2mM)}$ shows a ~0.6 eV positive shift of the rising edge from that of $MoFe\ protein^{FeMoco}$, implying a lesser degree of resemblance of this NifEN-bound "FeMoco" to the native cofactor in the MoFe protein.[5]

As their XAS spectra show, there is a considerable degree of similarity between the EXAFS data for $NifEN^{"FeMoco"(20mM)}$ and $MoFe\ protein^{FeMoco}$ in both frequency and beat pattern. The key beat region at $k = 10$ Å$^{-1}$ is conserved between the two species (Figure 3C), suggesting yet again that the Mo in $NifEN^{"FeMoco"(20mM)}$ is in a coordination environment similar to that in $MoFe\ protein^{FeMoco}$. The EXAFS intensity of $NifEN^{"FeMoco"(20mM)}$ is improved relative to that of $NifEN^{"FeMoco"(2mM)}$;[5] however, it is still diminished relative to that of $MoFe\ protein^{FeMoco}$ (Figure 3C). Additionally, the backscattering peak at ~5 Å, which corresponds to the distant, cross-cluster Mo−Fe backscattering in $MoFe\ protein^{FeMoco}$, is absent from the Fourier transform of $NifEN^{"FeMoco"(20mM)}$ (Figure 3D), suggesting that the Mo environment in $NifEN^{"FeMoco"(20mM)}$ is either

(7) Eady, R. R. *Chem. Rev.* **1996**, *96*, 3013–3030.
(8) Gangeswaran, R.; Eady, R. R. *Biochem. J.* **1996**, *317*, 103–108.
(9) Mayhew, S. G. *Eur. J. Biochem.* **1978**, *85*, 535–547.

***Table 1.*** Reconstitution of FeMoco-Deficient MoFe Protein by Various FeMoco Sources

| FeMoco source | activity [nmol (mg of protein)$^{-1}$ min$^{-1}$] | | | |
|---|---|---|---|---|
| | $C_2H_2$ formation under $C_2H_2$/Ar | $H_2$ formation under Ar | $NH_3$ formation under $N_2$ | $H_2$ formation under $N_2$ |
| $NifEN^{Precursor}$ | 0 | 0 | 0 | 0 |
| isolated FeMoco | 917 ± 105 | 1269 ± 154 | 305 ± 75 | 292 ± 20 |
| $NifEN^{"FeMoco"(20mM)}$ | 1065 ± 88 | 1100 ± 19 | 334 ± 40 | 323 ± 23 |
| $NifEN^{"FeMoco"[Ti(III)citrate]}$ | 680 ± 28 | 890 ± 35 | 272 ± 32 | 225 ± 9 |
| $NifEN^{"FeMoco"(Fld\_1)}$ | 538 ± 20 | 520 ± 21 | 210 ± 17 | 120 ± 5 |

less ordered or less symmetrical than that in MoFe $protein^{FeMoco}$. The high reconstitution activity of $NifEN^{"FeMoco"(20mM)}$ apparently points to the presence of a well-ordered Mo environment in NifEN-associated "FeMoco", in which the Mo is sufficiently secured in the "FeMoco" and therefore not easily lost during the transfer of "FeMoco" to the FeMoco-deficient MoFe protein. Moreover, despite their similarity, the "FeMoco" site in NifEN and the FeMoco site in the MoFe protein are different, particularly at the Mo end.[2] As such, it is very likely that Mo in NifEN-bound "FeMoco" has a somewhat different coordination than in the MoFe protein-bound FeMoco.

Indeed, in contrast to Mo in MoFe $protein^{FeMoco}$, which has three equidistant Fe backscatterers at 2.69 Å, Mo in $NifEN^{"FeMoco"(20mM)}$ can best be modeled by placing one Fe atom at 2.90 Å and the other two at 2.71 Å (Table 2), suggesting a slightly "off-center" coordination of Mo in $NifEN^{"FeMoco"(20mM)}$. Interestingly, $NifEN^{"FeMoco"(2mM)}$ does not have the Fe backscatterer at 2.90 Å.[5] This observation suggests a much stronger association of Mo and a more tightly organized Mo site in $NifEN^{"FeMoco"(20mM)}$. Further, compared with Mo in $NifEN^{"FeMoco"(2mM)}$, which has three O atoms at a consistently shorter average distance,[5] Mo in $NifEN^{"FeMoco"(20mM)}$ has one O at 2.12 Å and the other two at 2.24 Å, two of which are likely contributed by homocitrate. All of these Mo−O distances are longer than those in $NifEN^{"FeMoco"(2mM)}$ and more closely resemble the Mo−O coordination in MoFe $protein^{FeMoco}$ (Table 2). Finally, three S atoms can be modeled at an average distance of 2.37 Å to Mo in $NifEN^{"FeMoco"(20mM)}$, which is very similar to the three Mo−S distances in MoFe $protein^{FeMoco}$ (Table 2). Taken together, these results suggest an asymmetrical coordination of Mo in $NifEN^{"FeMoco"(20mM)}$ that is similar to the symmetrical one in MoFe $protein^{FeMoco}$. More importantly, $NifEN^{"FeMoco"(20mM)}$ has a much better Mo coordination than $NifEN^{"FeMoco"(2mM)}$, allowing the proposal of a model for the NifEN-bound "FeMoco" (Figure 3E).

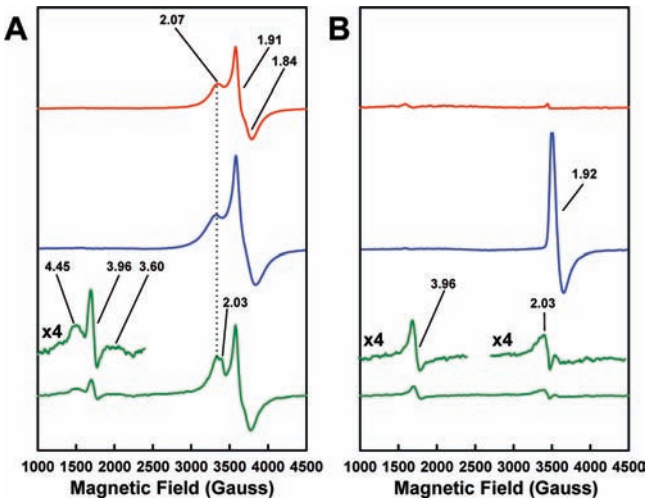


***Figure 2.*** EPR properties of Δ*nifB* NifEN (red), $NifEN^{Precursor}$ (blue), and $NifEN^{"FeMoco"(20mM)}$ (green) in (A) dithionite-reduced and (B) IDS-oxidized states. The dithionite-reduced samples were measured at 6 K, whereas the IDS-oxidized samples were measured at 15 K. The features of $NifEN^{"FeMoco"(20mM)}$ are enlarged, and the *g* values are indicated.

The combined outcome of these studies suggests that an increase in dithionite concentration results in a much tighter association of Mo to the NifEN-bound "FeMoco", allowing the observation of a FeMoco-like $S = {}^3/_2$ EPR signal and the modeling of a NifEN-bound "FeMoco" that adopts a conformation very similar to that of the MoFe protein-associated FeMoco. Such a reductant-dependence of FeMoco maturation is further exemplified by the ability of other nonphysiological reductants [e.g., Ti(III) citrate] and some physiological electron donors (e.g., flavodoxin 1 of *Azotobacter vinelandii*) to perform in the capacity of dithionite in FeMoco maturation (Figure 4; also see Figures S3 and S4 in the Supporting Information). $NifEN^{"FeMoco"}$ matured in the presence of 1.5 mM Ti(III) citrate (designated as $NifEN^{"FeMoco"[Ti(III)citrate]}$) or 40 μM reduced flavodoxin 1 (designated as $NifEN^{"FeMoco"(Fld\_1)}$) displayed the same characteristic EPR signals as those of $NifEN^{"FeMoco"(20mM)}$ in the dithionite-reduced (Figure 4A) and IDS-oxidized (Figure 4B) states. However, compared with $NifEN^{"FeMoco"(20mM)}$, both $NifEN^{"FeMoco"[Ti(III)citrate]}$ and $NifEN^{"FeMoco"(Fld\_1)}$ displayed EPR signals with reduced magnitudes and exhibited lower activities in the reconstitution assays (Table 1). The inability of Ti(III) citrate to completely mature the NifEN-bound precursor may originate from the harmful effect of this strong reductant on the integrity of NifEN and its associated clusters at higher concentrations, which is reflected by the sharp decrease in the reconstitution activity of $NifEN^{"FeMoco"[Ti(III)citrate]}$ when it was matured in >1.5 mM Ti(III) citrate (data not shown); in contrast, the suboptimal capacity of flavodoxin 1 in this process can be interpreted in terms of the "incorrect" redox potential of this electron donor (−330 mV[8]), which renders it less efficient in FeMoco maturation. The latter observation is particularly interesting in light of the optimal solution potential of dithionite for FeMoco maturation (ca. −440 mV, calculated for 20 mM dithionite[9]). More importantly, it suggests an essential role of redox chemistry in the in vivo process of FeMoco assembly. A solution potential of ca. −440 mV may produce a "correct" redox state of Mo before it can be mobilized by Fe protein, generate a particular redox state of the Fe protein that is favorable for Mo mobilization, or convert the NifEN-associated precursor to an optimal redox state for Mo attachment, all of which could account for the improved association of Mo to NifEN-bound "FeMoco". Further investigation along this line is in progress, and the optimal solution potential of dithionite will serve as a guideline for identifying in vivo electron donors for FeMoco maturation in the future.

(10) Schmid, B.; Ribbe, M. W.; Einsle, O.; Yoshida, M.; Thomas, L. M.; Dean, D. R.; Rees, D. C.; Burgess, B. K. *Science* **2002**, *296*, 352–356.

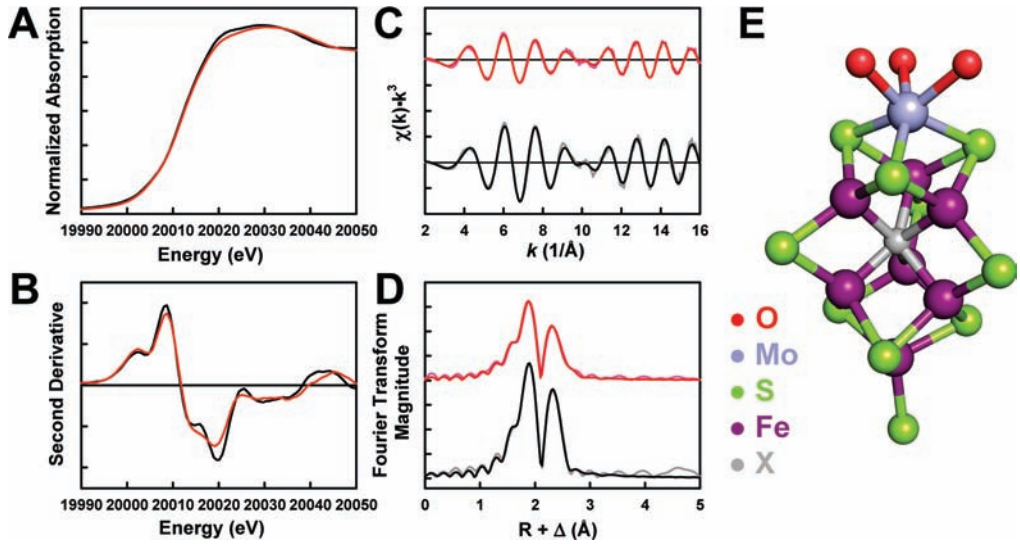


***Figure 3.*** (A) Mo K-edge XAS spectra and (B) smoothed second derivatives for NifEN$^{\text{"FeMoco"(20mM)}}$ (red) and MoFe protein$^{\text{FeMoco}}$ (black). (C) Mo K-edge EXAFS and (D) Fourier transforms of data (pink) and fits (red) for NifEN$^{\text{"FeMoco"(20mM)}}$ and data (gray) and fits (black) for MoFe protein$^{\text{FeMoco}}$. (E) Structural model of NifEN-bound "FeMoco". The structural model was adapted from the crystallographic coordinates of the MoFe protein[14] but modified for distances <3 Å from Mo on the basis of the EXAFS fits. S is shown as the ligand at the Fe end of the "FeMoco", as the Cys residue that ligates FeMoco in the MoFe protein is conserved in the NifE primary sequence.[2] The ligand at the Mo end of "FeMoco" is not given but is likely an Asn residue instead of the His ligand in the MoFe protein.[2]

***Table 2.*** Final EXAFS Fit Results over a *k* Range of 2−16 Å$^{-1}$ [a]

| | MoFe protein$^{\text{FeMoco}}$ | | | NifEN$^{\text{"FeMoco"(20mM)}}$ | | |
|---|---|---|---|---|---|---|
| scatterer | *N* | *R* (Å) | $\sigma^2$ (Å$^2$) | *N* | *R* (Å) | $\sigma^2$ (Å$^2$) |
| Mo−O short | − | − | − | 1 | 2.12 | 0.0055 |
| Mo−O long | 3 | 2.20 | 0.0053 | 2 | 2.24 | 0.0012 |
| Mo−S | 3 | 2.36 | 0.0022 | 3 | 2.37 | 0.0059 |
| Mo−Fe short | 3 | 2.69 | 0.0033 | 2 | 2.71 | 0.0029 |
| Mo−Fe long | − | − | − | 1 | 2.90 | 0.0058 |
| $\Delta E_0$ (eV) | | −11.0 | | | −8.9 | |
| weighted F | | 0.163 | | | 0.150 | |

[a] The variables are the coordination number, *N*, the interatomic distance, *R*, the mean-square thermal and static deviation, $\sigma^2$, and the shift in the threshold energy from 20 025 eV, $\Delta E_0$. The estimated uncertainties in *R*, $\sigma^2$ and *N* are ±0.02 Å, ±0.0001 Å$^2$, and ±20%, respectively. The goodness of fit, *F*, is defined as $F = [\sum k^6(\chi_{\text{exptl}} - \chi_{\text{calcd}})^2/\sum k^6(\chi_{\text{exptl}})^2]^{1/2}$.

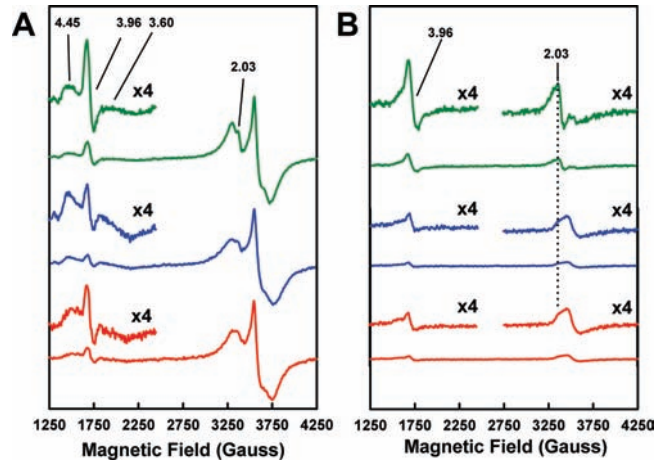


***Figure 4.*** EPR properties of NifEN$^{\text{"FeMoco"(20mM)}}$ (green), NifEN$^{\text{"FeMoco"[Ti(III)citrate]}}$ (blue), and NifEN$^{\text{"FeMoco"(Fld_1)}}$ (red) in (A) dithionite-reduced and (B) IDS-oxidized states. The dithionite-reduced samples were measured at 6 K, whereas the IDS-oxidized samples were measured at 15 K. The *g* values are indicated.

## 3. Experimental Procedures

**FeMoco Maturation.** The conversion of NifEN-bound precursor to "FeMoco" was performed in a 50 mL maturation assay containing 25 mM Tris-HCl (pH 8.0), 100 mg of NifEN$^{\text{Precursor}}$ (which was isolated from *A. vinelandii* strain DJ 1041[3]), 120 mg of the Fe protein, 0.4 mM homocitrate, 0.4 mM $Na_2MoO_4$, 2.4 mM ATP, 4.8 mM $MgCl_2$, 30 mM creatine phosphate, 24 units/mL creatine phosphokinase, and varying concentrations of dithionite ($Na_2S_2O_4$) (0, 2, 10, 20, and 40 mM) or Ti(III) citrate (0, 0.5, 1.5, 3, and 7.5 mM). In the case of *A. vinelandii* flavodoxin 1, 40 mg of reduced protein (i.e., a concentration of 40 $\mu$M) was added to the assay as a reductant to achieve a flavodoxin 1/NifEN molar ratio of 4:1. Reduced flavodoxin 1 of *A. vinelandii* was prepared by purifying the protein as described elsewhere[8] and removing excess dithionite by a single passage over a Sephadex G-50 column. In all cases, the maturation mixture was stirred for 1 h at 30 °C, after which NifEN was reisolated (categorically designated as NifEN$^{\text{"FeMoco"}}$) and used for reconstitution of FeMoco-deficient MoFe protein (see below). NifEN$^{\text{"FeMoco"(20mM)}}$ was examined further by EPR and XAS analyses (see below), whereas NifEN$^{\text{"FeMoco"[Ti(III)citrate]}}$ and NifEN$^{\text{"FeMoco"(Fld_1)}}$ were analyzed further by EPR only (see below). The purity of $Na_2S_2O_4$ (Sigma) was 85%, and the dithionite concentrations described above reflect the actual $Na_2S_2O_4$ content based on this purity.

**Reconstitution Analysis.** The reconstitution of MoFe protein was performed in a 0.8 mL assay containing 25 mM Tris-HCl (pH 8.0), 20 mM $Na_2S_2O_4$, and 0.5 mg of FeMoco-deficient Δ*nifB* MoFe protein (isolated from *A. vinelandii* strain DJ 1143[10]). FeMoco insertion was initiated with the addition of 2 mg of NifEN$^{\text{"FeMoco"}}$ to the assay, and the reaction mixture was then incubated for 30 min at 30 °C before termination and examination for enzymatic activities as described previously.[11]

**EPR Spectroscopy.** All of the samples for EPR spectroscopy were prepared in a Vacuum Atmospheres drybox (Hawthorne, CA) at an oxygen level of less than 4 ppm. Each sample contained 15 mg/mL protein, 10% glycerol, 2 mM $Na_2S_2O_4$, and 25 mM Tris-

(11) Ribbe, M. W.; Burgess, B. K. *Proc. Natl. Acad. Sci. U.S.A.* **2001**, *98*, 5521–5525.
(12) Tenderholt, A. *PYSPLINE*; Stanford Synchrotron Radiation Laboratory: Stanford, CA, 2006.

HCl (pH 8.0). The oxidized samples were prepared by incubating proteins with excess IDS for 30 min and subsequently removing IDS using an anion-exchange column. Spectra were collected in perpendicular mode using a Bruker ESP 300 $E_z$ spectrophotometer (Bruker, Billerica, MA) interfaced with an Oxford Instruments ESR-9002 liquid helium continuous-flow cryostat (Oxford Instruments, Oxford, U.K.). All of the spectra were recorded using a gain of $5 \times 10^4$, a modulation frequency of 100 kHz, a modulation amplitude of 5 G, and a microwave frequency of 9.62 GHz.

**XAS Data Acquisition.** XAS data were measured at the 20-pole wiggler BL7-3 biological XAS station at SSRL with storage ring parameters of 3 GeV and 80−100 mA. A premonochromator flat bent Rh-coated mirror provided rejection of higher harmonics and vertical collimation, and a Si(220) double-crystal monochromator was used for energy selection. Samples were stored in liquid nitrogen prior to data collection and held at a constant temperature of 10 K during data collection using an Oxford Instruments CF1208 liquid helium continuous-flow cryostat. A Canberra 30-element solid-state Ge detector array was used to record Mo K$\alpha$ fluorescence data. Through the use of Soller slits and a Zr filter secured between the sample cryostat and the detector window, signal intensity from inelastic scattering and Mo K$\beta$ fluorescence was substantially diminished. Internal energy calibration was performed by simultaneous measurement of the absorption of a Mo foil placed between two ionization chambers filled with Ar located after the sample. The first inflection point of the foil XAS edge was assigned to 20 003.9 eV. No signs of photoreduction of the metal sites, as observed by shifts in edge energy with time, were noted. A total of 38 and 12 scans were measured for NifEN$^{\text{"FeMoco"(20mM)}}$ and MoFe protein$^{\text{FeMoco}}$, respectively.

**XAS Data Analysis.** After inspection of raw data and averaging, the average data files for each sample were normalized using the program PYSPLINE[12] by fitting a second-order polynomial to the pre-edge region and subtracting from the entire data range with control points, followed by fitting a four-region spline function of orders 2, 3, and 3 over the post-edge region. The data were normalized to an edge jump of 1.0 at 20 025 eV. Though some data sets extended further, the data range selected for the EXAFS fits was limited to the shortest $k$ range (16 Å$^{-1}$) to ensure internally consistent fits. By means of the least-squares fitting program OPT, a component of the EXAFSPAK suite of software,[13] EXAFS data for $k = 2-16$ Å$^{-1}$ were fit using initial ab initio theoretical phase and amplitude functions calculated from FEFF 7.0[14] on the basis of the 1M1N[15] crystallographic starting model. Atomic coordinates from the crystal model were adjusted as necessary as fits were further refined. During fit optimization, the interatomic distance between the absorbing and backscattering atom ($R$) and the mean-square thermal and static deviation in $R$ ($\sigma^2$) were varied for all components. The threshold energy ($\Delta E_0$) was allowed to vary for each fit but constrained to the same value for all components. The amplitude reduction factor ($S_0^2$) was maintained at a value of 1.0 throughout analysis. Coordination numbers ($N$) were methodically adjusted from crystallographic values to provide the best chemically viable agreement to the EXAFS data and their Fourier transform. Inclusion or exclusion of various scattering paths was systematically tested to fully explore the atomic environment at Mo.

**Acknowledgment.** This work was supported by NIH Grants GM 67626 (M.W.R.) and RR 01209 (K.O.H.). SSRL operations are funded by the DOE BES, and the SSRL Structural Molecular Biology Program is funded by NIH NCRR BTP and DOE BER.

**Supporting Information Available:** Temperature-dependent EPR spectra. This material is available free of charge via the Internet at http://pubs.acs.org.

JA9035225

(13) George, G. N. *EXAFSPAK*; Stanford Synchrotron Radiation Laboratory: Stanford, CA, 1990.

(14) Rehr, J. J.; Albers, R. C. *Rev. Mod. Phys.* **2000**, *72*, 621–654.

(15) Einsle, O.; Tezcan, F. A.; Andrade, S. L. A.; Schmid, B.; Yoshida, M.; Howard, J. B.; Rees, D. C. *Science* **2002**, *297*, 1696–1700.